Calculation of the momentum density in ferromagnetic nickel

R. M. Singru* and P. E. Mijnarends
Reactor Centrum Nederland, Petten (N. H.), Netherlands
(Received 17 October 1973)

A band-structure calculation on the basis of Hubbard's approximation scheme has been made of the momentum-density distribution for positron annihilation and Compton scattering in ferromagnetic nickel. Graphs are shown of the contributions of the various bands for both spin directions, of the total momentum density, and of the spin density observable with polarized positrons. Owing to the symmetry of the wave functions the only pieces of Fermi surface observable with these techniques are the large sheets in the sixth majority- and minority-spin bands, and the minority-spin hole pocket in the third band. A comparison of the predicted angular correlation with experiment shows that the calculation somewhat overestimates the high-momentum region.

I. INTRODUCTION

Lately the momentum density in $3d$ transition metals is receiving increasingly more interest due to the present availability of strong positron and x-ray sources and to the use of γ rays in Compton-scattering experiments. Since in these metals the Fermi energy lies in or close to the $3d$ band, the Fermi surface often consists of a large number of pieces, which also in the extended-zone scheme are unconnected or multiply connected. Moreover the momentum-density contributions from the various electron bands will be strongly wave-vector dependent. A theoretical analysis of the momentum density is therefore indispensable if it is hoped to extract any useful information from the experimentally observed positron angular correlations[1] or Compton profiles.[2]

Various attempts have been undertaken to predict the momentum density in $3d$ metals, ranging from free-atom calculations combined with free-electron theory[3] via computations using the renormalized-atom model[4] to complete band-structure calculations.[5,6] Only in the latter type of calculation is it possible to take account of the Fermi-surface structure in a natural way. In the present paper a report is given of a band-structure calculation of the momentum density in nickel, both for Compton scattering and positron annihilation. Since for a proper understanding of the relation between band structure and momentum density, curves showing the total momentum density are of little value, the density distribution is broken down into its constituent parts corresponding to the core states and the six $3d$ and conduction bands for each spin direction. This also makes it possible to predict the spin density in momentum space which is observable with polarized positrons.

The computational method is essentially the same as that employed in a previous study of iron[5] and is briefly described in Sec. II. In Sec. III the results are presented in the form of momentum-density curves for Compton scattering and positron annihilation. In Sec. IV a comparison is made between the different band structures of nickel available in the literature.

II. CALCULATION

The momentum-density distribution of the photon pairs originating in the annihilation of thermalized positrons is given by[7]

$$\rho(\vec{p}) = \sum_{\vec{k},j} f(\vec{k},j) \left| \int e^{-i\vec{p}\cdot\vec{r}}\, \psi_{\vec{k},j}(\vec{r})\, \phi(\vec{r})\, d\vec{r} \right|^2 . \qquad (1)$$

Here $\vec{p}$ represents the momentum of the photon pair, $\psi_{\vec{k},j}(\vec{r})$ the wave function of the annihilated electron of wave vector $\vec{k}$ in the jth energy band, and $\phi(\vec{r})$ the wave function of the thermalized positron in its ground state $\vec{k}_+ = 0$. The function $f(\vec{k},j)$ gives the occupation of the state $(\vec{k},j)$ and is therefore related to the Fermi-Dirac function. Equation (1) also represents the momentum density derived from Compton scattering if $\phi(\vec{r})$ is replaced by unity. The experimentally observed profiles are related to Eq. (1) by integration of $\rho(\vec{p})$ with respect to one or two components of $\vec{p}$.

To calculate $\rho(\vec{p})$ from Eq. (1) requires the computation of the band structure $E_j(\vec{k})$ and the wave functions $\psi_{\vec{k},j}(\vec{r})$. This was done by means of the approximate method developed by Hubbard,[8] in which a secular equation of minimal size (9×9 for fcc metals) is computed from a given lattice potential. Solution of the resulting determinantal equation provides the eigenvalues $E_j(\vec{k})$, while the wave functions are obtained from the corresponding eigenfunctions. For a detailed description of this method the reader is referred to the original publications,[8,9] while the use of the wave functions to solve Eq. (1) is more fully discussed in Ref. 5.

The crystal potential employed in the numerical calculations is the self-consistent potential for ferromagnetic nickel as given by Wakoh.[10] The following values were taken for the lattice constant a, the radius r_i of the inscribed sphere, and the

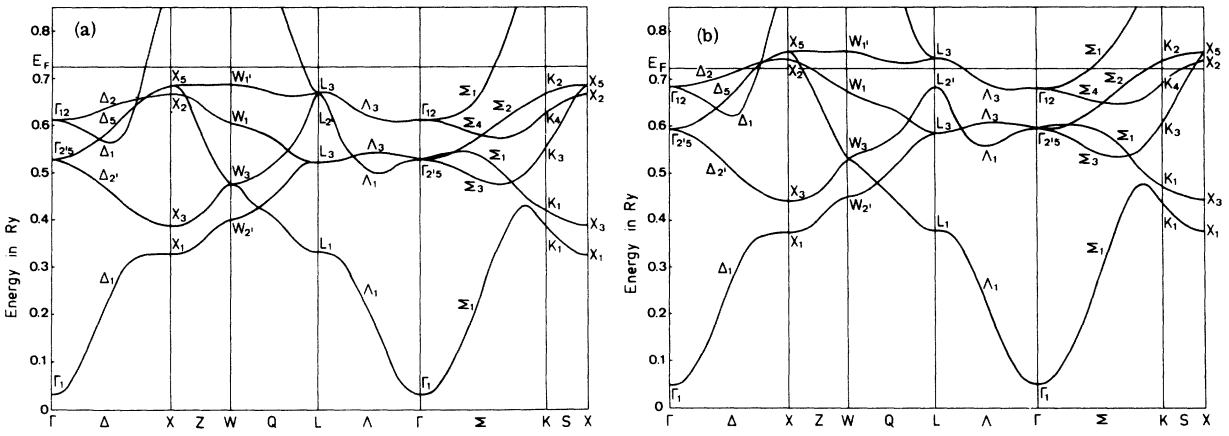

FIG. 1. Band structure for ferromagnetic nickel; (a) majority spin, (b) minority spin.

Wigner-Seitz radius r_s:

$$a = 6.65 \text{ a.u.} \quad r_i = 2.3511 \text{ a.u.}, \quad r_s = 2.5985 \text{ a.u.}$$

Our calculated band structure for the majority- (+) and minority- (−) spin states of nickel along some symmetry directions is shown in Figs. 1(a) and 1(b). There is good agreement between the present results and those of Wakoh; a comparison of 70 levels for each spin gave an rms error in the energy values of 0.010 Ry (0.009 Ry) for the + (−) spin bands. The main disagreement was that in our + spin bands the level at $L_{2'}$ lies deeper than L_3 by an amount +0.007 Ry, whereas Wakoh finds an energy difference of −0.009 Ry. The width of the d band ($X_5 - X_1$) in our band structure was 0.360 Ry (0.385 Ry) for the + (−) spin while the width of the overlapping s-p band ($X_{4'} - \Gamma_1$) was 0.856 Ry for the + as well as the − spin.

The positron wave function $\phi(\vec{r})$ was calculated using a plane-wave expansion,

$$\phi(\vec{r}) = \frac{1}{\tau^{1/2}} \sum_{\vec{K}} A_{\vec{K}} e^{i\vec{K}\cdot\vec{r}}, \tag{2}$$

similar to Gould *et al.*[11] The secular equation

$$\sum_{\vec{K}} [(K^2 - E)\delta_{\vec{K}\vec{K}'} + V_{\vec{K}-\vec{K}'}] A_{\vec{K}} = 0 \tag{3}$$

was written in a symmetrized form and solved using the Fourier coefficients

$$V_{\vec{K}-\vec{K}'} = (1/\tau) \int_\tau V(r) e^{i(\vec{K}-\vec{K}')\cdot\vec{r}} d\vec{r} \tag{4}$$

calculated from the minority-spin potential. Partial waves up to $l = 12$ were used in evaluating $V_{\vec{K}-\vec{K}'}$ by expansion of Eq. (4). The number of plane waves used in the expansion [Eq. (2)] was 89 (7 shells) and this calculation resulted in a positron energy equal to 0.548 Ry with respect to the constant potential in the interstitial region. Increasing the number of plane waves from 89 to 259 did not cause any appreciable change in the eigenvalue or the Fourier coefficients $A_{\vec{K}}$. Following Gould *et al.*, the first Fourier coefficient was adjusted so that $\phi(\vec{r} = 0) = \tau^{-1/2} \sum_{\vec{K}} A_{\vec{K}} = 0$, subject to the normalization condition $\sum_{\vec{K}} |A_{\vec{K}}|^2 = 1$.

The entire procedure was checked by calculating the positron wave function in aluminum employing the crystal potential by Segall.[12] The results agreed reasonably well with those of Stroud and Ehrenreich.[13] Figure 2 shows the positron wave function in nickel by the present calculation for the three crystal directions ⟨100⟩, ⟨110⟩, and ⟨111⟩. For the subsequent computations of $\rho(\vec{p})$ the part of the positron wave function inside the inscribed sphere was spherically averaged according to[14]

$$\phi(r) = \tfrac{1}{35}[10\phi_{100}(\vec{r}) + 16\phi_{110}(\vec{r}) + 9\phi_{111}(\vec{r})]. \tag{5}$$

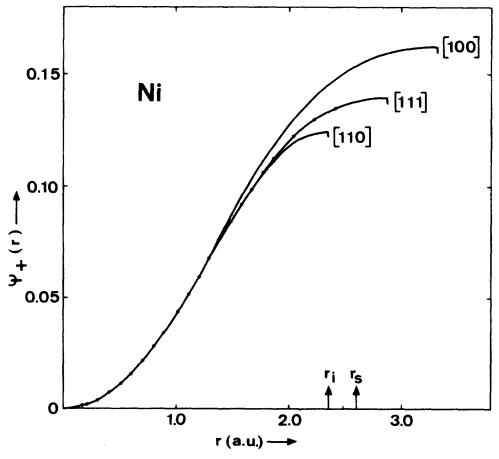

FIG. 2. Positron wave function for nickel for three symmetry directions. The dots represent the spherically averaged part of the positron wave function inside the inscribed sphere used in the calculation of $\rho(\vec{p})$.

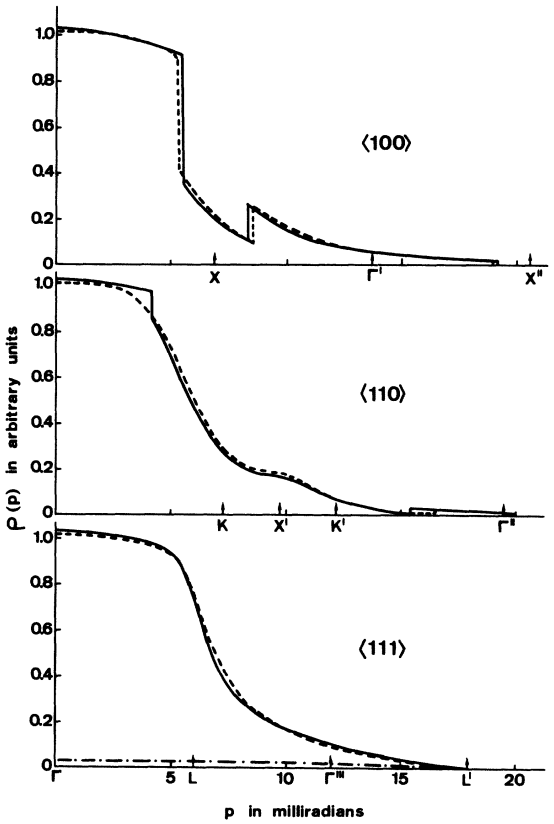

FIG. 3. The calculated two-photon momentum density $\rho(\vec{p})$ from the $3d$ and conduction band for the two spin directions of ferromagnetic nickel along the ⟨100⟩, ⟨110⟩, and ⟨111⟩ directions in momentum space. The solid lines refer to the majority spin, the dashed lines to the minority spin. The momentum p is expressed in mrad. The chain curve in the ⟨111⟩ graph shows the isotropic contribution to $\rho(\vec{p})$ by the core ($1s$, $2s$, $2p$, $3s$, $3p$) electrons.

The momentum density $\rho_c(\vec{p})$ of the core electrons was assumed to be isotropic and was calculated from the equation[15]

$$\rho_c(p) = 4\pi \sum_{n,l} (2l+1) \left| \int_0^{r_s} j_l(pr) R_+(r) P_{nl}(r) r^2 dr \right|^2, \qquad (6)$$

where $j_l(pr)$ is the spherical Bessel function, $R_+(r)/r$ is the spherically averaged positron wave function and $P_{nl}(r)/r$'s are the free-atom orbital wave functions for nickel as given by Herman and Skillman.[16] The summation in Eq. (6) was carried out for the $1s$, $2s$, $2p$, $3s$, and $3p$ orbitals. In evaluating the integral (6) a correction for the proper region of integration was made following Berko and Plaskett.[15] All calculations were carried out on a CDC-6600 computer.

III. RESULTS

The two-photon momentum densities for the two spin populations which resulted from these calculations are shown in Fig. 3. They are expressed in arbitrary units which remain unchanged throughout the paper. The momentum density shows most structure along the cube axes, viz., a wide gap centered on X at 6.9 mrad for both spin populations. The curves are rather similar to those obtained earlier for copper.[5] The main difference is found in the ⟨110⟩ directions where the discontinuity at the Fermi surface in the sixth majority-spin band is much smaller in nickel than in copper. This is a result of the hybridization of this band with the highest $3d$ band of Σ_1 symmetry. Since in nickel the Fermi level intersects the hybridized band at a smaller wave number than in copper the wave function still possesses most of its original $3d$ character, which means that its contribution to the momentum density will behave as p^4 at low wave numbers (and not as p^2 as stated in Ref. 5). The same holds to an even larger extent for the corresponding – spin band, where the discontinuity at the Fermi surface has become unobservably small.

Together with the ⟨111⟩ curves the isotropic core contribution is shown, stemming from the $1s, \ldots, 3p$ electrons. This contribution is relatively small compared with that of the band electrons because the Coulomb repulsion excludes the positron from the core region. Even so, the core contribution may appear unexpectedly low, but it should be kept in mind that Fig. 3 shows the momentum density $\rho(\vec{p})$, and that the double integration effected by the commonly used long-slit angular-correlation apparatus still has to be carried out. Since the core contribution extends up to high values of momentum and since these are weighted by a factor p, the relative importance of the core electrons will be increased in going from $\rho(\vec{p})$ to the angular correlation.

The momentum densities summed over all bands do not provide much insight in the way in which they depend on the occupation of the individual bands. Yet, such an insight is needed to predict the effect of small changes in the band structure in the vicinity of the Fermi level, or the effect of changes in the Fermi level with respect to otherwise rigid bands by alloying. For that purpose a series of graphs is shown in Figs. 4 and 5 which present the contributions of the individual bands, both for the + and – spin direction, as contour diagrams in the extended zone scheme. The various sheets of the + and – spin Fermi surfaces are clearly visible. Also shown are the lines along which bands of different representations touch. On these lines a transfer of momentum density takes place between neighboring bands since, as has been shown elsewhere,[5] only bands belonging to the totally symmetric representation of the group of the wave vector $\vec{k}$ can give a nonzero contribution to

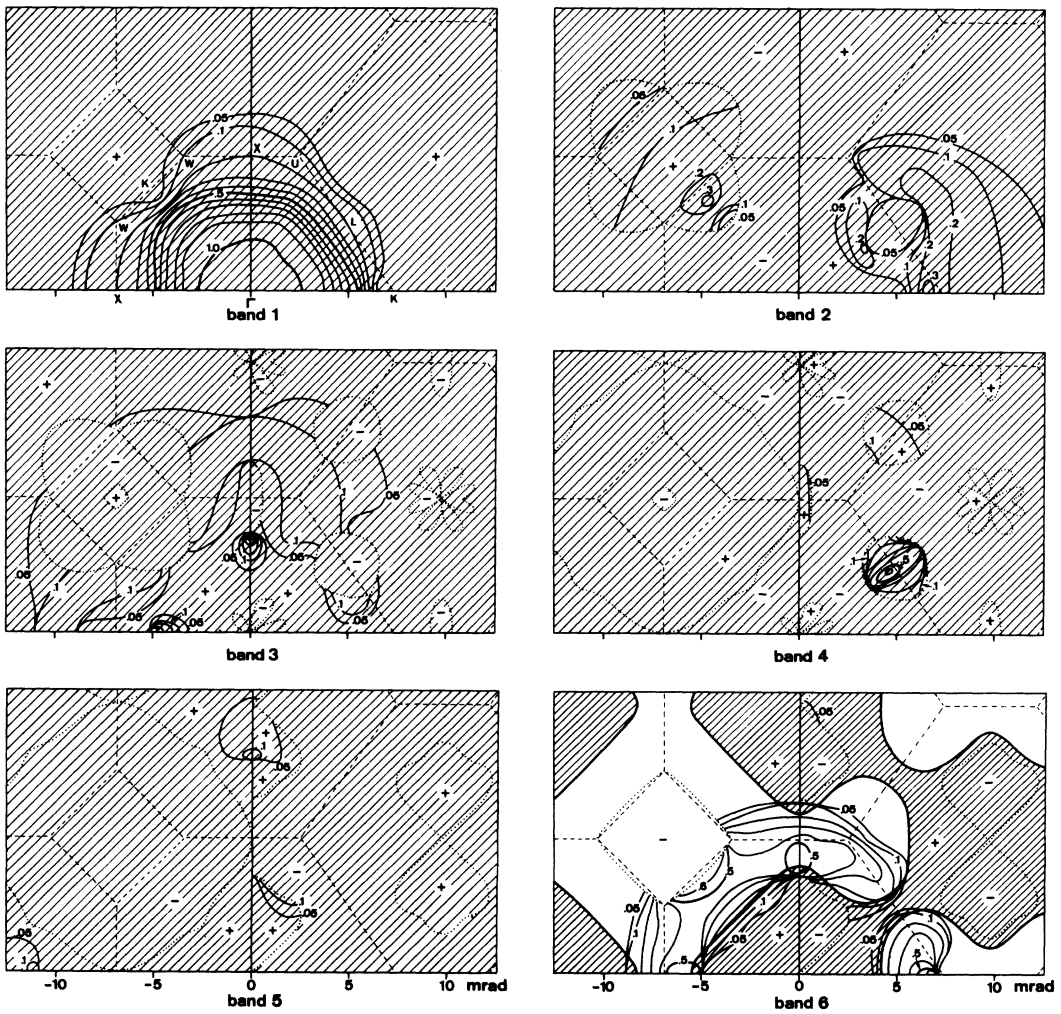

FIG. 4. Contribution of the majority-spin 3*d* and conduction bands to the photon pair momentum density in the (100) plane (left) and (110) plane (right) in nickel. The bands are numbered from the bottom (Fig. 1). Dotted curves indicate the lines along which bands touch while broken lines represent the Brillouin zone boundaries. The shaded areas correspond to $\vec{k}$ states occupied by electrons. The plus and minus signs refer to the representation of the wave functions.

the momentum density in the first Brillouin zone. (In the higher Brillouin zones, where $\vec{p}=\vec{k}+\vec{K}$ with $\vec{K}$ a vector of the reciprocal lattice, the contributing bands can be found with the aid of the selection rule given in Ref. 5.) Possibly there may also be a transfer of density between neighboring bands of the same representation which approach each other closely, as is the case with the lowest two Σ_1 bands near K. The deficiency in density in band 1 near K is compensated by a small peak in the same region in the second band. It is uncertain, however, whether this is a real effect or caused by an incomplete diagonalization of the secular determinant for these two nearly degenerate bands. A close scrutiny of the graphs furthermore reveals that the momentum densities in the various bands are very little spin dependent, which is not surprising for two sets of more or less rigid bands split by the exchange interaction. From these graphs it also becomes clear now that the ⟨100⟩ curves in Fig. 3 are somewhat misleading. Whereas for the + spin electrons the gap at X is caused by the large, multiply-connected electron sheet in the sixth band, the gap for the other spin direction originates in the hole pockets in band 3⁻. Consequently, when moving along a radius a few degrees off the ⟨100⟩ direction one still crosses the + spin Fermi surface (although the drop in momen-

tum density at this surface rapidly decreases as the radius is rotated away from the ⟨100⟩ axis), while the discontinuity in the − spin momentum density disappears for angles larger than 7°. A further discussion of these graphs will be deferred until Sec. IV, where they will be reconsidered in connection with a discussion of a number of band structures published by various authors.

If a nickel single crystal is magnetically saturated along the direction of an incoming beam of polarized positrons the two-photon angular correlation will depend on the direction of magnetization. This enables one to study the momentum-density distributions of the two spin populations separately. In practice this is most easily done by deriving the difference (called the spin density) and the sum of the two distributions. Figure 6 shows the predicted spin density $\Delta\rho(\vec{p}) = \rho_+(\vec{p}) - \rho_-(\vec{p})$ along the ⟨100⟩, ⟨110⟩, and ⟨111⟩ directions. Its most striking feature is the negative region between 4–5 and 12–15 mrad, a result of the exchange polarization, i.e., spin dependence of the electronic wave functions. It is remarkable that, with exception of the ⟨110⟩ direction, there seems to be very little spin density in the high-momentum region above say 14 mrad, in contrast with iron where the umklapp processes give relatively large contributions which also have been found experimentally.[17] The positive peak at 16 mrad in the ⟨110⟩ direction is caused by the difference in the Fermi radii k_{110} between the large sheets centered on the reciprocal-lattice point (2, 2, 0) in the sixth

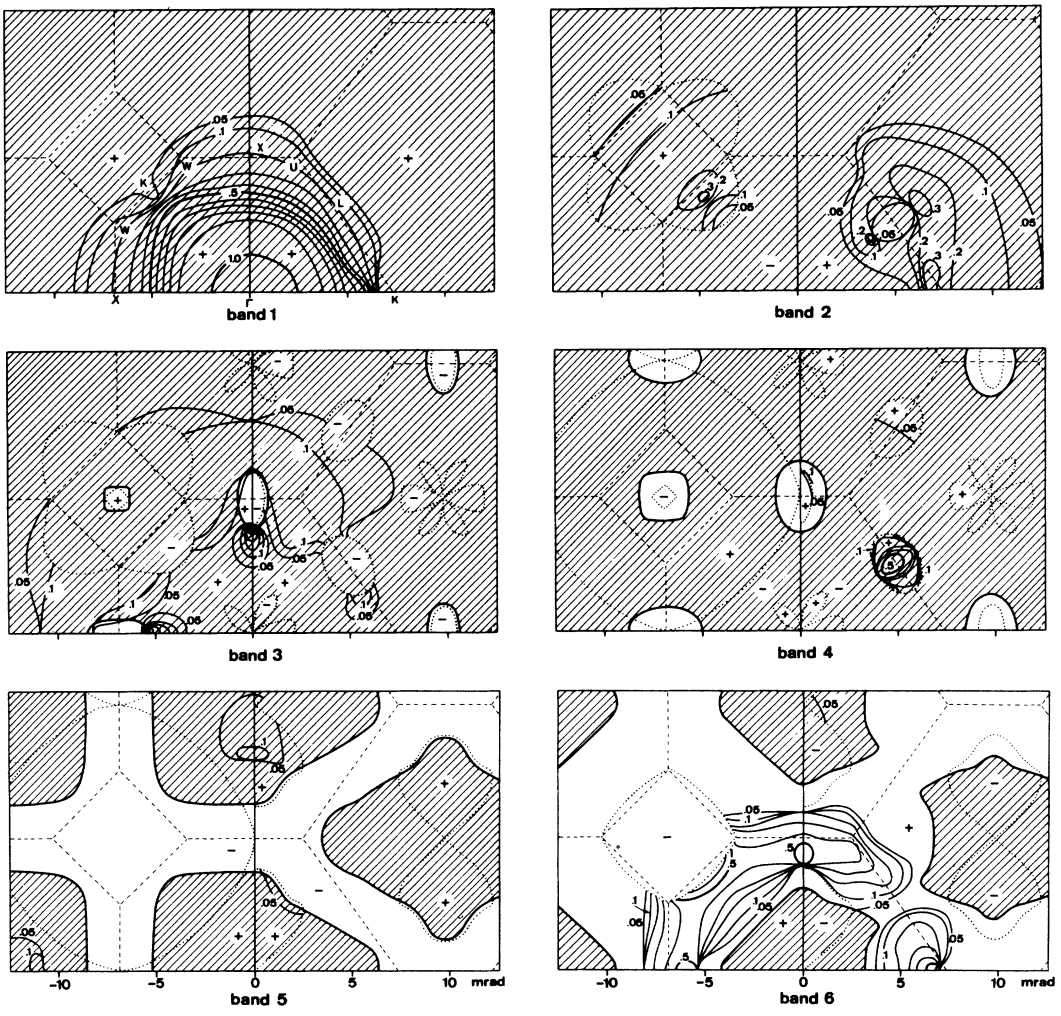

FIG. 5. Same as Fig. 4 but for minority spin.

majority- and minority-spin bands. Since both surfaces have rather flat faces perpendicular to the ⟨110⟩ axis there should be clear breaks at 15.2 and 16.3 mrad even in an experiment employing a conventional long-slit geometry. Observations of these breaks would constitute the first measurement of these Fermi radii. Similar breaks may be expected in a long-slit experiment at 5.5 and 6.6 mrad, and at 12.9 and 14.0 mrad, originating from the corresponding sheets centered on (2, 0, 0) and (0, 2, 0). Measurements of the difference angular correlation $\Delta N(p_z) = \int\int \Delta\rho(\vec{p})dp_x dp_y$ have been reported by various authors. The data of Berko and Mills, [18] corrected for the 3γ effect, show a negative region for $p_z \lesssim 8$ mrad with fairly large high-momentum components (HMC) for the ⟨100⟩ and ⟨111⟩ directions; a ⟨110⟩ curve is not shown. The results of Mihalisin and Parks[19–21] are difficult to compare with the present work because they are given in the form of $P(p_z) = \Delta N(p_z)/N(p_z)$. Recent measurements by Shiotani *et al.*[22] show a null effect along ⟨100⟩, and a negative region upto $p_z \sim 10$ mrad followed by positive HMC. These HMC could be due to the region of positive spin density $\Delta\rho$ around 16 mrad discussed above.

It would be most attractive to use the computed momentum densities as a starting point for a calculation of the long-slit angular correlations for a number of crystal orientations. The two-dimensional integration, however, requires the momentum density to be known on a mesh throughout all of momentum space. As the computational effort involved in this seemed excessive, we have limited ourselves to an approximate calculation of the angular correlation for a polycrystalline Ni sample. To this end the momentum density was spherically averaged by writing it as a sum of the three curves of Fig. 3 with the same coefficients as Eq. (5). After addition of the core contribution $\rho_c(p)$ use was made of the relation

$$N(p_z) = \int_{|p_z|}^{\infty} \rho_{\text{sph av}}(p)pdp. \tag{7}$$

The resulting curve is shown in Fig. 7, together with experimental data on Ni single crystals by Shiotani *et al.*[22] The latter curve represents an average of the data for the [100] and [110] directions and field up and down, and has been normalized to the calculated value at $p_z = 0$ mrad. Data on a [111] Ni single crystal of Berko and Mills[18,23] show a good general agreement with the curve of Shiotani *et al.* The calculated curve agrees well with the experimental data up to about 5 mrad, but it lies slightly higher at larger angles. Apparently the calculation somewhat overestimates the high-momentum region. A similar discrepancy has been observed in iron.[24]

In addition to the band-electron momentum density for positron annihilation we have also calculated the corresponding quantity for Compton scattering. The results are shown in Fig. 8. Within the first Brillouin zone there is hardly any difference between the positron and Compton results, but at high momenta the density for Compton scattering is much higher. This reflects the absence of the positron wave function which reduces the contributions of the core orbitals. From this density distribution the *band-electron* Compton profile, shown in Fig.

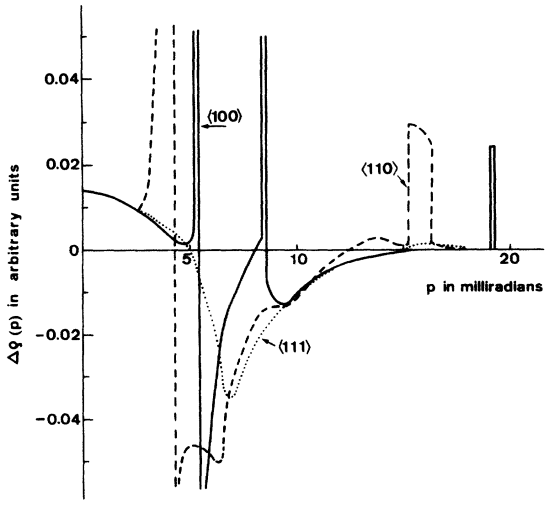

FIG. 6. The calculated spin density $\Delta\rho(\vec{p})$ (3*d* and conduction band only) according to the band structure of Fig. 1.

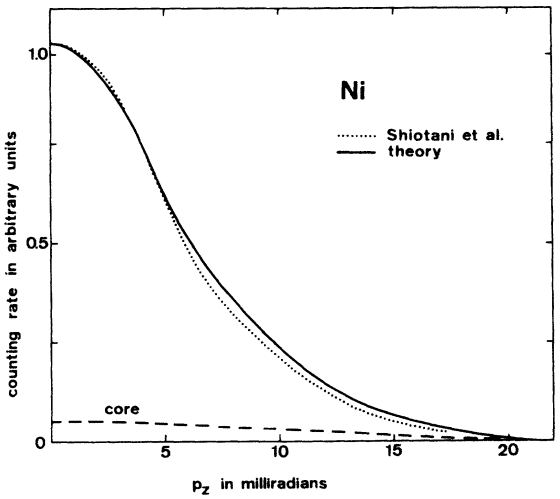

FIG. 7. Comparison between the calculated and experimental angular correlation curves for polycrystalline nickel. The theoretical curve (solid line) was calculated using the $\rho(\vec{p})$ curves from Fig. 3 after addition of the $1s^2$, ..., $3p^6$ core contribution which is also shown separately by the dashed curve.

9, has been computed in the manner described above [Eq. (7)]. A comparison with the positron angular correlation in the same graph (Fig. 9) shows that not only is the Compton scattering amplitude higher at high momenta, but also the full width at half-maximum (FWHM) of the curve is appreciably larger. Also this is a result of the large high-momentum content of the Compton momentum-density distribution.

IV. RELATION TO BAND STRUCTURE

The band structure of ferromagnetic nickel has been the subject of many studies. Wakoh[10] and Connolly[25] made self-consistent calculations using the Korringa-Kohn-Rostoker (KKR) and augmented-plane-wave (APW) techniques,[26] respectively. Hodges, Ehrenreich, and Lang[27] and Zornberg[28] made use of an interpolation scheme which they fitted to the results of *ab initio* calculations for paramagnetic Ni. By subsequently including spin-orbit and exchange interactions and making small adjustments of the constants in their model Hamiltonian they obtained semiempirical band structures which gave good agreement with the available experimental data. More recently, Langlinais and Callaway[29] performed a tight-binding calculation, which was made self-consistent by Callaway and Wang.[30] The *ab initio* calculations all give essentially similar results for the band structure and the resulting Fermi surface on those points which can be studied by positron annihilation and Compton scattering. The interpolation method of Hodges *et al.* places the − spin $L_{2'}$ level above the Fermi level, thereby creating a hole pocket at L in addition to the − spin hole pockets at X. Moreover, they mention the possible existence of + spin hole pockets at X and W in view of the uncertainty in the exact location of the X_2, X_5, and $W_{1'}$ levels with respect to the Fermi level. Since the $L_{2'}$ level is a p-like level there is a high peak of density associated with it as can be seen in Fig. 5. This makes the pocket, if it exists, in principle observable with positrons or Compton scattering. The + spin pockets cannot be observed because the bands eventually responsible for them have the wrong symmetry. So far none of these pockets have been detected in de Haas–van Alphen (dHvA) experiments except for the − spin hole pocket at X in band 4.[28,31] Actually the only other piece of Fermi surface observed through the dHvA effect is the neck of the multiply-connected sheet in band 6^+. Neither the large sheets in bands 5^- and 6^- nor the hole pocket in band 3^- have as yet been found.

The self-consistent calculation of Connolly has been performed for two values of the exchange potential, viz., the full free-electron exchange and this exchange potential reduced by a factor of $\frac{2}{3}$.

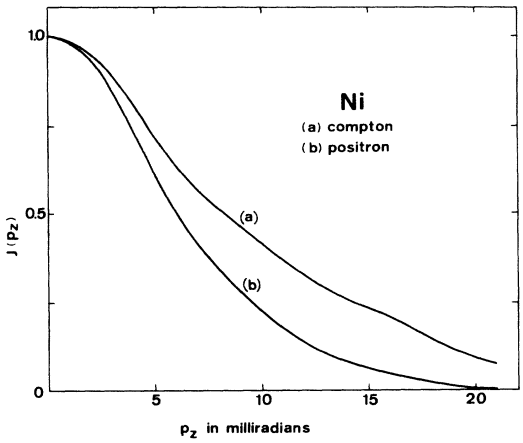

FIG. 9. Comparison of the band profiles for (a) Compton scattering and (b) positron annihilation. The profiles were calculated from Eq. (7) using $\rho(\vec{p})$ from Figs. 3 and 8. The curves have both been normalized at $p=0$.

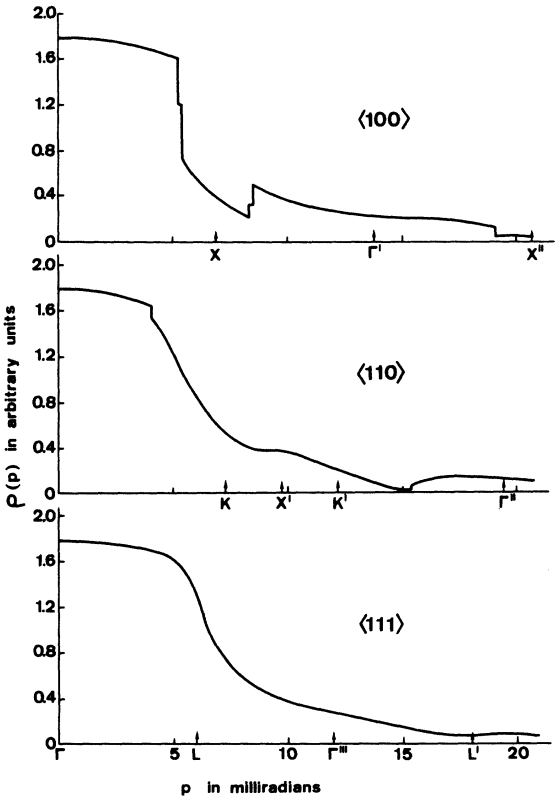

FIG. 8. Calculated momentum density for Compton scattering from nickel along the ⟨100⟩, ⟨110⟩, and ⟨111⟩ directions. The curves show the sum contribution of the majority- and minority-spin electrons in the 3*d* and conduction bands.

Use of the full exchange potential gave a much smaller s-d separation than the reduced potential. As a result the + spin Fermi surface in band 6 was found to be closed instead of multiply connected, in contradiction with the dHvA observations of the neck. The band structure obtained with the reduced exchange potential is in general agreement with the results of the present work and it is expected that this band structure will give rise to a momentum-density distribution very similar to that shown in Figs. 4–6. In other words, although there are small differences like the relative position of the + spin $L_{2'}$ and L_3 levels (Connolly: $L_{2'} - L_3 \sim 0.01$ Ry, present work: $L_{2'} - L_3 = -0.007$ Ry) positron annihilation and Compton scattering are not sensitive to them.

Zornberg's band structure, obtained by fitting the parameters in Mueller's interpolation scheme to a number of experimental data, cannot very well be compared with the results of the present work because he includes the spin-orbit interaction. However, one of his results deserves some comment. In the course of dHvA studies[32] it has been observed that the hole pocket in band 4^- changes volume when the magnetic field is rotated with respect to the crystalline axes. The reason is that in the presence of spin-orbit coupling the magnetic field lowers the originally cubic symmetry of the crystal. This effect will not be observable with positrons or Compton scattering, however, because from Fig. 5 it is seen that according to the present calculation there is little or no momentum density present at the surface of this pocket, partly due to the wave-function symmetry and partly due to the d character of the Z_1 band. This conclusion does not depend on the details of the band structure because a careful analysis of the other band structures along the same lines shows that there never is any appreciable momentum density around X in the fourth band.

The band structures resulting from the calculation of Langlinais and Callaway and that of Callaway and Wang are in good agreement with each other, although they were obtained for different values of α, the reduction coefficient of the exchange potential. They also agree closely with Connolly's structure except for the crossing of the – spin Δ_1, Δ_2, and Δ_5 bands. As a result the small part of the density peak at the end of the 3^- band hole pocket now shifts to the 5^- band, while the rest of the peak remains in the 3^- band. Thus it depends on the band structure whether the gap at X along the $\langle 001 \rangle$ directions is related to the 3^- hole pocket or the 5^- sheet. Thus a measurement of the width of this gap will not provide unique information on this part of the Fermi surface unless the band structure in the neighborhood of X is accurately known.

The present work has shown once more that in metals with partly filled d bands, wave-function symmetry plays a most important role in determining which parts of the band structure and the Fermi surface are accessible to study by positron annihilation or Compton scattering. An approach in which to every sheet of the Fermi surface an average momentum density is assigned will therefore be unable to reproduce the observed angular correlations or line profiles, as demonstrated by the work of Shiotani *et al.*[22] The only sheets about which one can expect to obtain information by these experimental techniques are the large sheets in the sixth minority- and majority-spin bands, and possibly a small part of the sheet in the 5^- band. Since the dimensions of these sheets are not accurately known yet by other techniques, positron annihilation and the Compton-line-profile method can make a useful contribution. The information obtainable about the hole pocket in band 3^- probably depends too much on small details of the band structure as to be of much value.

ACKNOWLEDGMENTS

One of us (R. M. S.) wishes to express his gratitude to Reactor Centrum Nederland for its kind hospitality. We are indebted to Dr. N. Shiotani and his co-workers for sending us their results prior to publication and to Professor S. Berko for making his data available to us.

*Present address: Department of Physics, Indian Institute of Technology, Kanpur (U. P.) 208016, India.

[1] *Positron Annihilation*, edited by A. T. Stewart and L. O. Roellig (Academic, New York, 1967).
[2] M. Cooper, Adv. Phys. 20, 453 (1971).
[3] R. J. Weiss, Phys. Rev. Lett. 24, 883 (1970).
[4] K.-F. Berggren, Phys. Rev. B 6, 2156 (1972).
[5] P. E. Mijnarends, Physica (Utr.) 63, 235 (1973).
[6] F. M. Mueller, B. N. Harmon, D. D. Koelling, and A. J. Freeman, Bull. Am. Phys. Soc. 18, 364 (1973).
[7] S. de Benedetti, C. E. Cowan, W. R. Konneker, and H. Primakoff, Phys. Rev. 77, 205 (1950).
[8] J. Hubbard, J. Phys. C 2, 1222 (1969).
[9] J. Hubbard and P. E. Mijnarends, J. Phys. C 5, 2323 (1972).
[10] S. Wakoh, J. Phys. Soc. Jap. 20, 1894 (1965).
[11] A. G. Gould, R. N. West, and B. G. Hogg, Can. J. Phys. 50, 2294 (1972).
[12] B. Segall, Phys. Rev. 124, 1797 (1961).
[13] D. Stroud and H. Ehrenreich, Phys. Rev. 171, 399 (1968).
[14] D. D. Betts, A. B. Bhatia, and M. Wyman, Phys. Rev. 104, 37 (1956).
[15] S. Berko and J. S. Plaskett, Phys. Rev. 112, 1877 (1958).
[16] F. Herman and S. Skillman, *Atomic Structure Calcu-*

lations (Prentice-Hall, Englewood Cliffs, N. J., 1963).
[17]P. E. Mijnarends, Physica (Utr.) 63, 248 (1973).
[18]S. Berko and A. P. Mills, J. Phys. (Paris) 32, C1-287 (1971).
[19]T. W. Mihalisin and R. D. Parks, Phys. Lett. 21, 610 (1966).
[20]T. W. Mihalisin and R. D. Parks, Phys. Rev. Lett. 18, 210 (1967).
[21]T. W. Mihalisin and R. D. Parks, Solid State Commun. 7, 33 (1969).
[22]N. Shiotani, T. Okada, H. Sekizawa, T. Mizoguch and T. Karasawa, J. Phys. Soc. Jap. 35, 456 (1973).
[23]S. Berko (private communication).
[24]W. C. Phillips and R. J. Weiss, Phys. Rev. B 6, 4213 (1972).
[25]J. W. D. Connolly, Phys. Rev. 159, 415 (1967).
[26]*Methods in Computational Physics*, edited by B. Alder, S. Fernbach, and M. Rotenberg (Academic, New York, 1968), Vol. 8.
[27]L. Hodges, H. Ehrenreich, and N. D. Lang, Phys. Rev. 152, 505 (1966).
[28]E. I. Zornberg, Phys. Rev. B 1, 244 (1970).
[29]J. Langlinais and J. Callaway, Phys. Rev. B 5, 124 (1972).
[30]J. Callaway and C. S. Wang, Phys. Rev. B 7, 1096 (1973).
[31]D. C. Tsui, Phys. Rev. 164, 669 (1967).
[32]L. Hodges, D. R. Stone, and A. V. Gold, Phys. Rev. Lett. 19, 655 (1967).